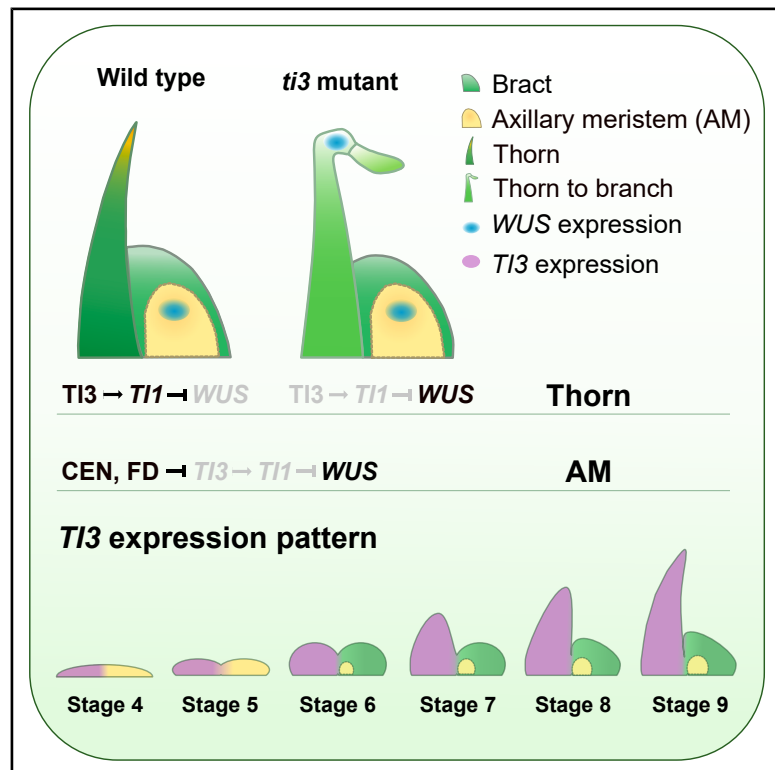


Thorn specification in citrus plants by an SHI/STY family transcription factor

Graphical abstract



Authors

Qingyou Zheng, Shiyun Zhou,
Vivian F. Irish, Fei Zhang

Correspondence

feizhang@mail.hzau.edu.cn

In brief

Zheng et al. find that the SHI/STY family transcription factor THORN IDENTITY3 (*T13*) specifies thorn fate by activating *T1* and *T2*, which in turn repress *CsWUS* to promote determinate growth. In the adjacent axillary meristem, however, the *CsCEN*-*CsFD* complex represses *T13*, thereby sustaining *CsWUS* expression and maintaining stem cell activity.

Highlights

- *T13* encodes an SHI/STY family transcription factor that specifies thorn identity
- *T13*, expressed in thorn primordia, directly activates thorn identity genes *T1*/*2*
- *CsCEN*, expressed in axillary meristem, represses *T13* to maintain stem cell activity
- *T13* homologs in other Rutaceae species likely regulate thorn specification

Article

Thorn specification in citrus plants by an SHI/STY family transcription factor

Qingyou Zheng,^{1,2} Shiyun Zhou,^{1,2} Vivian F. Irish,^{3,4} and Fei Zhang^{1,2,5,*}

¹National Key Laboratory for Germplasm Innovation & Utilization of Horticultural Crops, College of Horticulture & Forestry Sciences, Huazhong Agricultural University, Wuhan 430070, Hubei, China

²Hubei Hongshan Laboratory, Wuhan 430070, Hubei, China

³Department of Molecular, Cellular and Developmental Biology, Yale University, New Haven, CT 06520, USA

⁴Department of Ecology and Evolutionary Biology, Yale University, New Haven, CT 06520, USA

⁵Lead contact

*Correspondence: feizhang@mail.hzau.edu.cn

<https://doi.org/10.1016/j.cub.2026.01.002>

SUMMARY

Thorns are modified branches that have evolved independently multiple times as defenses against herbivores. We previously identified the TCP transcription factors THORN IDENTITY1 (TI1) and TI2 as key regulators of thorn development in *Citrus*; however, how these genes are regulated remains unclear. In this study, using comparative transcriptomics, we identified *TI3*, encoding a SHORT INTERNODES/STYLISH (SHI/STY) family transcription factor that is specifically expressed in thorns. We found that *TI3* binds to a previously undefined CTAG core element in the promoters of *TI1* and *TI2*, activating their expression to promote stem cell arrest in the thorn meristem. CRISPR-Cas9-mediated disruption of *TI3* function converted thorns into branches. Conversely, the PEBP family protein CsCENTRORADIALIS (CsCEN) represses *TI3* expression in the axillary meristem to maintain stem cell activity and promote branch development. Mutations in CsCEN resulted in branch-to-thorn conversions, whereas *cscen ti3* double mutants exhibited the *ti3* mutant phenotype, supporting the idea that CsCEN regulates *TI3* expression. The thorn-specific expression pattern of *TI3* homologs across three Rutaceae species suggests that *TI3* might have a conserved role in thorn development. Thus, *TI3* represents a new regulator of meristem identity, and manipulating its activity is a promising approach for breeding thornless cultivars.

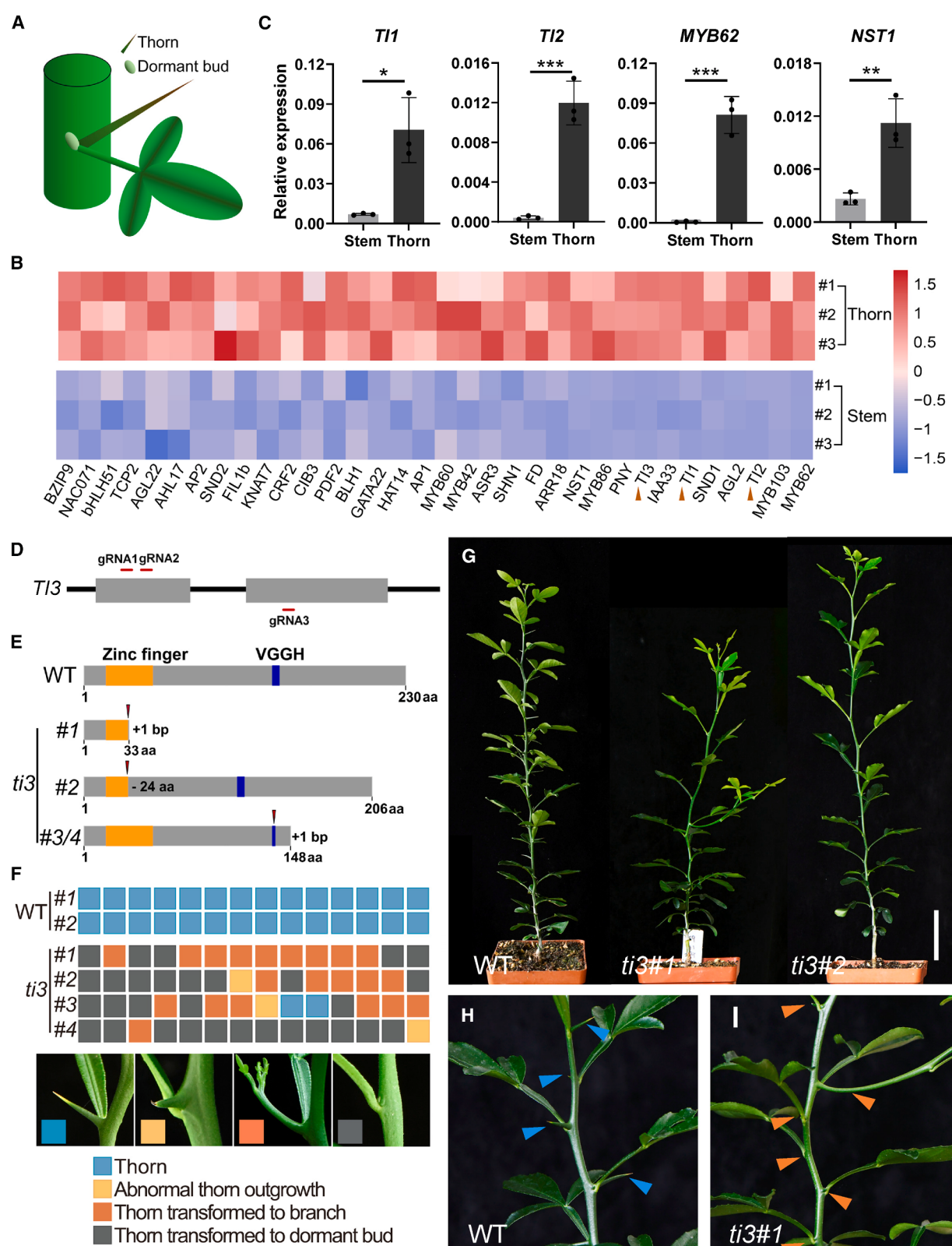
INTRODUCTION

In plants, stem cell proliferation and arrest are critical for organ initiation and functional specification.¹ Stem cells reside in specialized regions termed meristems, and their activity relies on WUSCHEL (WUS)-related homeobox (WOX) transcription factors.² The shoot apical meristem (SAM) and root apical meristem (RAM), located at opposite poles of angiosperm plants, are indeterminate meristems that maintain stem cell activity and establish shoot and root architectures, respectively.³ By contrast, determinate meristems, such as those forming leaves and flowers, maintain stem cell activity transiently before undergoing arrest.^{4,5}

Thorns, modified branches that protect plants from herbivores, develop from determinate axillary meristems (AMs).⁶ Unlike indeterminate AMs that produce branches, *Citrus* thorn meristems (TMs) terminate stem cell activity, coincident with the repression of CsWUS. Our previous work identified TCP transcription factors THORN IDENTITY1 (TI1) and TI2 as key repressors of CsWUS.⁷ Mutations in *TI1* and *TI2* convert thorns into branches. Adjacent to the TM lies a dormant AM, where CsWUS expression is maintained through CsCENTRORADIALIS (CsCEN)-mediated repression of *TI1*.⁸ This spatial regulation of meristem fate and rapid thorn differentiation alongside branch meristem dormancy shapes juvenile citrus tree architecture.⁹

However, the mechanisms initiating TMs and activating the *TI* genes remain unknown.

The SHORT INTERNODES/STYLISH (SHI/STY) family of transcription factors regulates diverse processes, including internode elongation, gynoecium development, lateral root formation, and photomorphogenesis.^{10–14} In *Arabidopsis thaliana*, this family comprises 10 members—SHI, STY1/2, SHI-RELATED SEQUENCE (SRS)3–8, and LATERAL ROOT PRIMORDIUM1 (LRP1). These regulators act largely through auxin signaling. For instance, STY1, STY2, SHI, SRS5, and LRP1 collectively promote auxin biosynthesis in gynoecium marginal tissues, while these five members redundantly specify anther identity via direct activation of *YUCCA* genes and other genes like *POLYAMINE OXIDASE5*, *ENHANCER3 OF DA1*, and *PECTIN LYASE-LIKE1*.¹⁵ The role of SHI/STY genes in reproductive development is conserved, as evidenced by their requirement for archegonial differentiation in the moss *Physcomitrium patens*.¹⁶ Individual members can confer distinct functions. SRS5 promotes photomorphogenesis by activating *ELONGATED HYPOCOTYL5*, *B-BOX PROTEIN21* (BBX21), and BBX22, while auxin signaling represses SRS5 via *AUXIN RESPONSE FACTOR7/9* to facilitate lateral root development.^{17,18} Beyond *Arabidopsis*, SHI/STY genes regulate nodule emergence in legumes,¹⁹ wood formation in poplar,²⁰ nectary development in *Aquilegia*,²¹ and inflorescence architecture in



(legend on next page)

grasses.^{22,23} In rice, OsSHI1 interacts with IDEAL PLANT ARCHITECTURE1 (IPA1) to downregulate *TEOSINTE BRANCHED1* (*OsTB1*) and *DENSE AND ERECT PANICLE1*, thereby increasing rice tillering but reducing panicle size.²² In barley, the grass-specific SHI/STY gene *Six-rowed spike 2* (*Vrs2*) controls floral organ patterning and phase duration.²³

Despite extensive characterization of this family, the function of SRS3 remains undefined. Here, we demonstrate that *Citrus SRS3* promotes thorn specification—hence its redesignation as *THORN IDENTITY3* (*Ti3*). *Ti3* directly activates *T11* and *T12* expression in thorn primordia. Conversely, in AMs, *CsCEN* represses *Ti3* to sustain stem cell activity. The specific expression of *Ti3* homologs in thorn-bearing species suggests a possible conserved role for SRS3 in thorn evolution.

RESULTS

Ti3 terminates stem cell activity of TM

To identify genes regulating thorn development, we compared transcriptomes from dissected young stems and thorns (stages 9–11) of *Poncirus trifoliata* (Figure 1A; Data S1). We identified 34 transcription factor genes preferentially expressed in developing thorns (Figure 1B). Among these were the thorn identity genes, *T11* and *T12*, along with genes involved in thorn-tip sclerification, *MYB62* and *NST1*.^{7,24} Quantitative real-time PCR validated the RNA sequencing (RNA-seq) results for these genes (Figure 1C), confirming that our approach captured genes involved in both thorn identity determination and terminal differentiation.

We then performed a CRISPR-Cas9 screen in Carrizo citrange (*Citrus sinensis* “Washington” sweet orange \times *P. trifoliata*) to test the remaining candidates. Among the 34 thorn-enriched genes, nine (*T11*, *T12*, *MYB103*, *MYB62*, *SND1*, *NST1*, *SHN1*, *MYB42*, and *BLH1*) had been knocked out in previous studies.^{7,24} We designed 1–2 guide RNAs (gRNAs) to target each remaining gene individually and succeeded in knocking out eight genes, with at least two fully knockout lines for each gene (Figures S1A–S1H; Data S2). This screen revealed a novel thorn identity gene, *Ti3*, which encodes an SHI/STY family transcription factor. In the screen, two gRNAs (gRNA1 and gRNA2) targeting the first exon of *Ti3* produced two fully edited lines (lines 1 and 2) (Figures 1D and 1E). Loss-of-function *ti3* mutants exhibited a thorn-to-branch conversion phenotype, with thorns developing into branches or dormant buds (Figures 1F–1I). Notably, AM growth was unaffected and remained dormant in both wild-type (WT) and *ti3* mutants. To confirm this phenotype, a third gRNA (gRNA3) targeting a conserved I/VGGH domain yielded

two additional independent fully edited lines (lines 3 and 4), which displayed the same mutant phenotype (Figures 1E, 1F, and S1I–S1L), demonstrating the specific role of *Ti3* in promoting thorn development.

Scanning electron microscopy (SEM) analysis revealed no obvious differences between WT and *ti3* mutants at each leaf axil until stage 6. At stage 7, pointed thorn primordia were evident in WT, while axillary bud-like structures appeared at the corresponding positions in the mutant (Figures 2A and 2B). In mutants, bracts became overgrown (Figures 2C–2E). As development proceeded, active branches or dormant buds formed at the presumed thorn position for most nodes in mutants (Figures 2F–2H), indicating that *Ti3* acts early to specify thorn fate.

We next analyzed the *CsWUS* expression. *CsWUS* was detected in AMs of both WT and *ti3* (stages 7–9; Figures S1M–S1R), with no signal from sense-probe controls (Figures S1S and S1T). In WT thorn primordia, *CsWUS* expression was present until stage 7 but absent by stage 8 and later (Figures 2I, 2K, and 2M). By contrast, *CsWUS* expression persisted in the thorn-converted branch primordia of *ti3* mutants from early stages through stage 9 (Figures 2J, 2L, and 2N). This result demonstrates that *Ti3* is required to terminate stem cell activity in the TM.

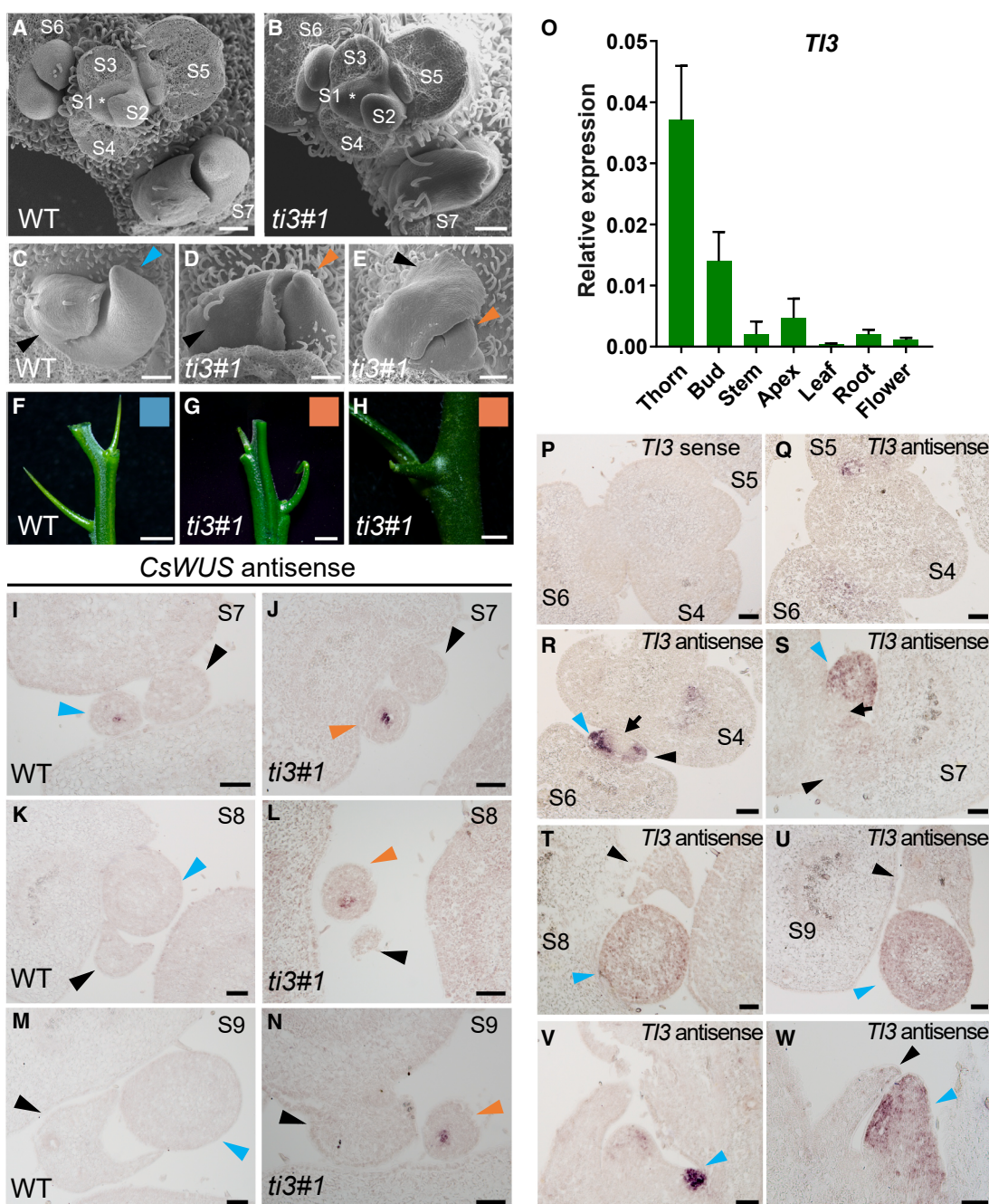
Ti3 is an *AtSRS3* homolog specifically expressed during thorn development

Through surveying the sweet orange genome (*C. sinensis*, v2.0), we identified four additional SRS/STY family genes alongside *Ti3*. A maximum-likelihood phylogenetic tree was constructed using the amino acid sequences of these five *C. sinensis* members along with the putative homologs from *Arabidopsis thaliana*, *Lotus japonicus*, *Populus trichocarpa*, *Aquilegia coerulea*, and rice (Figure S2A). *Ti3* clusters with *AtSRS3* and related SRS proteins from *Populus* and *Lotus*, whose functions remain unclear. *Ti3* protein localized to the nucleus (Figure S2B).

Quantitative real-time PCR showed that *Ti3* transcripts were abundant in young thorns (~0.5 cm), axillary buds, and shoot apices but undetectable in flowers, leaves, and roots (Figure 2O). We performed *Ti3* RNA *in situ* hybridization using shoot apices of seedlings (Figures 2P–2W). *Ti3* expression was first detected in the TM at stage 4 and persisted throughout subsequent stages within the thorn primordia (Figures 2Q–2U). Longitudinal sections revealed broad expression across the developing thorn (Figures 2V and 2W). *Ti3* expression was also detected in the bract primordia at early stages (Figure 2R). By contrast, no signal was detected in stems, the SAM, leaf

Figure 1. *Ti3* is required for thorn identity in *Citrus*

- (A) Schematic illustrating the positions of the thorn and AM at the nodal region.
- (B) Heatmap of 34 differentially expressed transcription factor genes (stems versus thorns, \log_2 fold change ≤ -1 and adjusted $p < 0.01$). Thorn identity genes are highlighted with brown arrowheads.
- (C) Quantitative real-time PCR validation of *T11*, *T12*, *MYB62*, and *NST1* in stems versus thorns of *Poncirus trifoliata*. Error bars represent means \pm SD ($n = 3$ biological replicates). * $p < 0.05$, ** $p < 0.01$, *** $p < 0.001$ (Student's *t* test).
- (D) Genomic structure of the *Ti3* showing the coding sequence (thick bar) and target sites of three guide RNAs (gRNA1–3, red bars).
- (E) Mutations in the *Ti3* gene. Protein domains are highlighted: zinc finger (orange) and VGGH (blue). Mutation sites are marked by red arrowheads. Indicated are a +1 bp insertion causing a frameshift (lines 1, 3, and 4) and a 24-amino acid deletion disrupting the zinc-finger domain (line 2). aa, amino acids.
- (F) Thorn position fate analysis. Each square represents the growth type at the sequential nodal thorn positions from the plant base to apex. Blue, thorn; yellow, abnormal thorn outgrowth; orange, thorn-to-branch; gray, thorn-to-dormant bud.
- (G–I) Mutation of *Ti3* converts thorns into branches. Blue arrowheads, thorns; orange arrowheads, thorns-to-branches. Scale bars, 5 cm.
- See also Figures S1 and S2 and Data S1 and S2.



T13 antisense

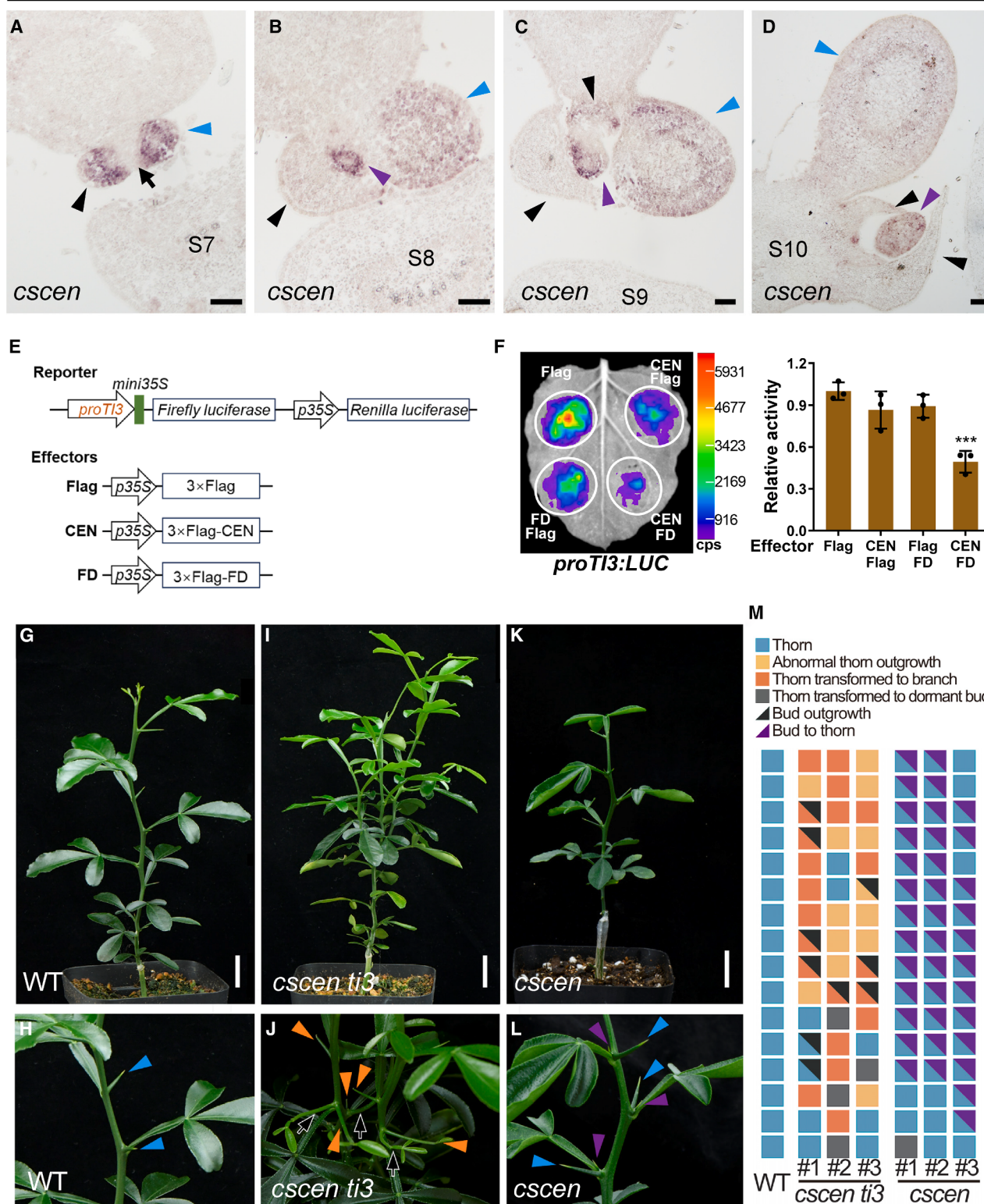


Figure 3. *CsCEN* represses *T13* to prevent ectopic thorn development

(A-D) RNA *in situ* hybridization for *T13* on cross-sections of *cscen* mutants at stage 7 (A), 8 (B), 9 (C), and 10 (D). Blue arrowheads, thorn primordia; black arrowheads, bracts; purple arrowheads, dormant buds transformed into thorns; black arrow, AM. Scale bars, 50 μ m.

(legend continued on next page)

primordia, or AMs. The sense-probe control showed no signal (Figure 2P). The specific expression pattern in thorns and bracts aligns with the mutant phenotype of these organs.

CsCEN maintains AM identity by repressing *Ti3* expression

The absence of *Ti3* expression in the AM prompted us to investigate its relationship with CsCEN, which specifically expressed within AM.⁸ In *cscen* mutants, dormant AMs develop into thorns, producing a double-thorn phenotype at each leaf axil. We analyzed *Ti3* expression in *cscen* mutants via RNA *in situ* hybridization. Transcripts were detected in the branch-to-thorn conversion primordia from stage 8 onward in *cscen* mutants, whereas no expression was observed in WT AMs at equivalent stages (Figures 3A–3D). These results suggest that CsCEN represses *Ti3* expression in AM.

To determine the mechanism of repression, we performed dual-luciferase assays via transient expression in *Nicotiana benthamiana* leaves. Since CsCEN typically acts with FD, we tested the effect of the CsCEN-CsFD complex on a 2.3-kb *Ti3* promoter. Co-expression of CsCEN and CsFD strongly repressed *proTi3:LUC* reporter activity, whereas neither protein alone had this effect (Figures 3E and 3F). Thus, the CsCEN-CsFD protein complex represses *Ti3* promoter activity to maintain AM identity.

To define the genetic relationship between CsCEN and *Ti3*, we generated three *cscen ti3* double mutants. Unlike the double-thorn phenotype of *cscen* mutants, all *cscen ti3* double mutants produced two branches per leaf axil, phenocopying the *ti3* single mutants (Figures 3G–3M). This genetic evidence confirms that CsCEN acts upstream of *Ti3* to promote an indeterminate fate in the AM.

Ti3 activates the expression of *Ti1* and *Ti2*

To identify potential downstream targets of Ti3, we performed transcriptome profiling using the *ti3* single mutant and *cscen ti3* double mutants (Data S3). Comparison of *ti3* mutants with WT identified 169 differentially expressed genes (DEGs) ($|\log_2 \text{fold change}| \geq 0.5$, adjusted $p < 0.05$) (Figure 4A). Of these, 38 genes were also differentially expressed in the *cscen ti3* double mutants compared with WT ($|\log_2 \text{fold change}| \geq 0.5$, adjusted $p < 0.05$) (Figure S3A). This overlapping set included nine transcription factor genes, among them the known genes *Ti1*, *Ti2*, *MYB62*, and *NST1* (Figure S3B). *Ti3* itself was also significantly downregulated in *ti3*. Quantitative real-time PCR analysis confirmed the reductions of *Ti1*, *Ti2*, and *Ti3* transcripts in *ti3* (Figure 4B), supporting that *Ti1* and *Ti2* act downstream of *Ti3*.

We next tested whether Ti3 can regulate the promoters of *Ti1* and *Ti2*. Previous studies showed that STY1-clade proteins bind to two similar *cis* elements, ACTCTAC/A or T/GCTCTAC.^{12,22} We

identified one such motif in the 2.4-kb *Ti1* promoter (*proTi1*) and two in the 2.1-kb *Ti2* promoter (*proTi2*) (Figure S3C). In transient expression assays, while Ti3 alone led to a slight increase in LUC activity, a Ti3-VP64 fusion (fused with VP64 strong activation domain²⁵) activated the *proTi2:LUC* reporter (Figures S3D and S3E). Conversely, a Ti3-SRDX fusion (fused with SRDX transcriptional repressor²⁶) strongly repressed it. Ti3-VP64 fusion also activated the *proTi1:LUC* reporter significantly (Figures S3F and S3G). These results indicate that Ti3 can regulate *Ti1*/*Ti2* promoters but may require co-factor(s) for full activity.

To determine if the predicted STY1-binding motifs are necessary for Ti3 function, we generated truncated promoter fragment reporters containing the motifs (854 bp with one motif for *proTi1F1* and 942 bp with two motifs for *proTi2F1*) and created mutated versions, *proTi1F1(m):LUC* and *proTi2F1(m):LUC*. Surprisingly, Ti3 activated both WT and mutated promoters to similar levels (Figures S3F–S3I). This indicates that Ti3, as a member of the SRS3 clade, does not depend on the canonical STY1-binding motifs for its activity on these promoters, and it may bind alternative sequences or function through a distinct mechanism.

Ti3 binds to CTAG core motifs in the promoters of *Ti* genes

We mapped genome-wide Ti3-binding sites using DAP-seq analysis. This identified 2,945 significant peaks ($q < 0.05$), with 46.99% located within promoter regions (<3 kb from transcriptional start site) and 0.27% in 3' UTRs (<0.3 kb after the stop codon) (Figure 4C; Data S4). *De novo* motif analysis of peak summits revealed a strongly enriched motif, CTAG ($p = 1e-698$) (Figure 4D; Data S5). We identified a single Ti3-binding peak in the *Ti1* promoter containing five copies of CTAG, while two peaks in the *Ti2* promoter contained two and six copies (Figures 4E and 4F).

To validate Ti3 binding to these CTAG motifs, we generated luciferase reporters driven by WT promoter fragments containing the peaks, control fragments without the motif, and mutated versions where the CTAG repeats were disrupted (Figure 4G). Co-expression with 35S::Ti3-VP64 in transactivation assays showed that Ti3-VP64 significantly activated the *proTi1P:LUC* reporters (peak, T2, and T3) but not the reporters without a binding site (T1) or with the mutated version (T3m) (Figure 4H). Similarly, for the *Ti2* promoter, activation was only observed for the reporters containing CTAG motifs (for Peak1, Peak1 and T2; for Peak2, Peak2, T1, and T2) (Figures 4I and 4J). The RING-like zinc-finger domain was crucial for this regulation, as a Ti3 mutant sequence with a disrupted zinc-finger domain (~24 aa) completely lost the ability to activate *Ti1/2* promoters (Figure S4). We employed electrophoretic mobility shift assays (EMSA) to confirm direct binding *in vitro*. Recombinant GST-Ti3 fusion proteins caused a band shift only when incubated with Ti1P, Ti2P1, and Ti2P2

(E and F) CsCEN represses the *Ti3* promoter.

(E) Schematic of reporter and effector constructs. *Mini35S*, a 60-bp 35S minimum promoter element.

(F) Transient expression assays in *Nicotiana benthamiana* leaves. Error bars represent means \pm SD ($n = 3$ biological replicates). *** $p < 0.001$ (Student's *t* test).

(G–M) Genetic interaction between CsCEN and *Ti3*.

(G–L) Phenotypes of WT (G and H), *cscen ti3* (I and J), and *cscen* (K and L) mutants grafted onto WT rootstock. Scale bars, 2 cm.

(M) Nodal-fate analysis of the first 16 nodes of WT and three independent mutant lines.

Color code for (G)–(M): blue, thorn; yellow, abnormal thorn; orange, thorn-to-branch; gray, thorn-to-dormant bud; black, dormant bud-to-branch; purple, dormant bud-to-thorn.

See also Data S2.

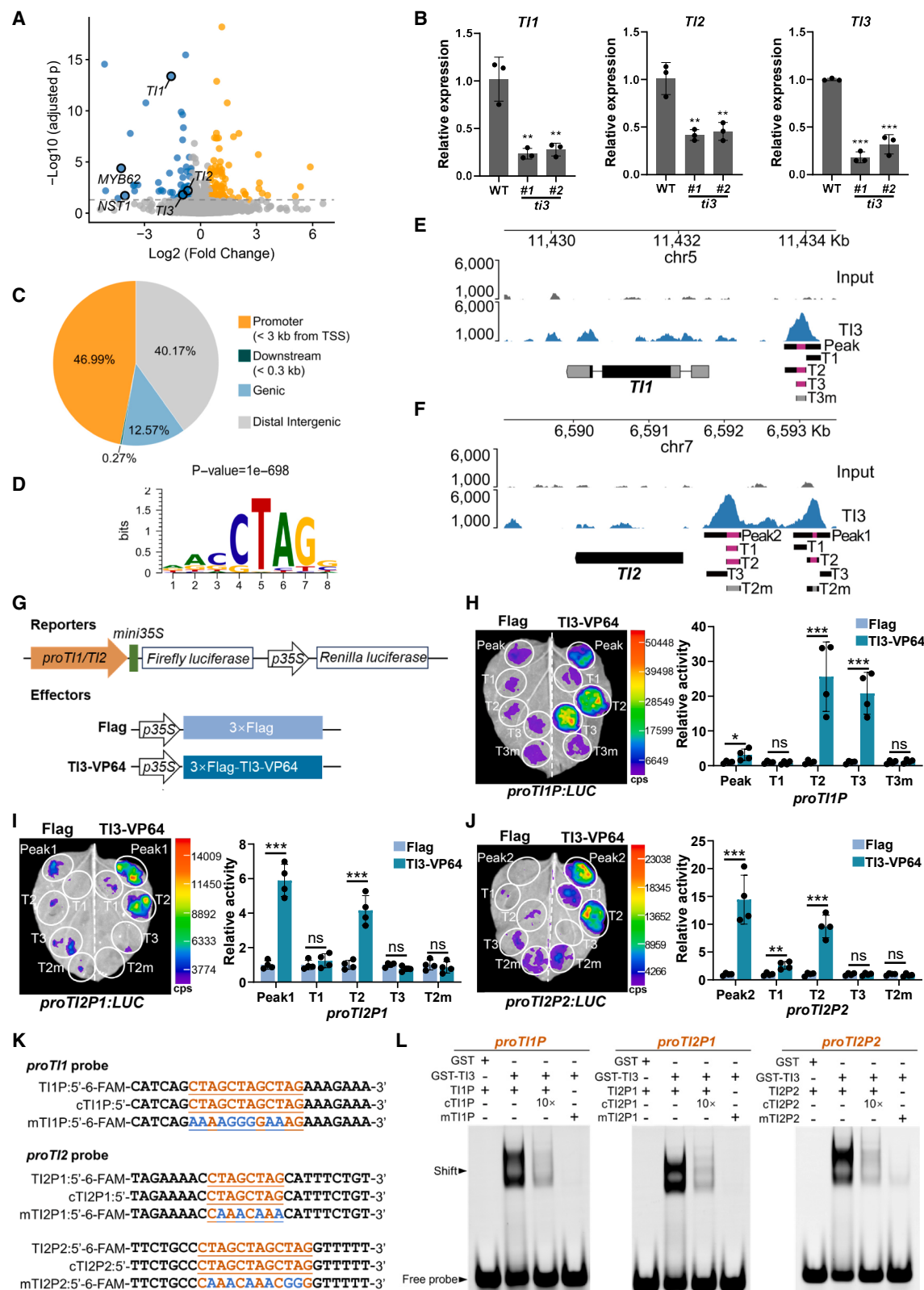


Figure 4. TI3 directly promotes the expression of *TI* genes by binding to CTAG motifs

(A) Volcano plot of DEGs between WT and *ti3* mutants from RNA-seq analysis of young shoots (~0.5 cm apices containing SAM, young leaves, young thorns, stems, and axillary buds). *TI1*, *TI2*, *TI3*, *MYB62*, and *NST1* are highlighted.

(legend continued on next page)

probes but not with the mutant probes (mTi1P, mTi2P1, and mTi2P2). This shift was effectively competed away by a 10-fold excess of unlabeled probe (Figures 4K and 4L). These results demonstrate that Ti3 directly regulates *Ti1* and *Ti2* expression by binding to tandem CTAG motifs in their promoters.

We also identified two Ti3-binding peaks within its own locus: one in the upstream promoter (with one CTAG) and one in the 3' UTR (with five CTAG copies) (Figure 5A). Transient activation assays showed that Ti3-VP64 did not activate the *Ti3* upstream promoter (*proTi3P1*) (Figures 5B and 5C) but strongly activated a reporter driven by the 3' UTR fragment (*proTi3P2*: Peak2 and T2) (Figure 5D). EMSAs confirmed specific binding of the Ti3 protein to the Ti3P2 probe, while no band shift occurred with the mutant control mTi3P2 (Figures 5E and 5F). Furthermore, probes with increasing numbers of CTAG motifs produced a slower-migrating shift, indicating multimeric, copy-number-dependent binding (Figure 5G). These results indicate that Ti3 positively autoregulates its expression by binding to a high-affinity site containing tandem CTAG repeats in its 3' UTR.

***Ti3* acts in the same genetic pathway as *Ti1* and *Ti2* to specify thorn fate**

Having established that Ti3 directly regulates *Ti1* and *Ti2*, we examined their genetic interactions. *Ti1* and *Ti2* are *BRC1/2* homologs, known to regulate axillary bud dormancy,^{7,27,28} whereas *Ti3* is preferentially expressed in TM and does not affect AM outgrowth. The *ti1* single mutants exhibited abnormal thorn outgrowth, with approximately 2 of 14 thorns converted into branches. A higher defect frequency was observed in *ti1 ti3* double mutants, where the majority of thorns (~11 of 14 nodes) were transformed into branches or remained as dormant buds (Figures S5A–S5F). In *ti1 ti2 ti3* triple mutants, nearly all thorns (~13 of 14 nodes) were converted into branches or buds, closely resembling that of *ti1 ti2* double mutants. Additionally, dormant AMs developed into branches (~5 of 14 nodes) in *ti1 ti2 ti3* mutants (Figures S5G–S5K), similar to that in *ti1 ti2* mutants, which is attributed to the role of *BRC* genes in bud dormancy. These results indicate that *Ti3* functions within the same genetic pathway as *Ti1* and *Ti2* in controlling thorn identity.

***Ti3* shows a conserved function in specifying thorn identity**

Thorns are common in Rutaceae species. We selected three representative species: the Australian finger lime (*Citrus*

australisica, known for its prominent thorns), Chinese box orange (*Atalantia buxifolia*), and lime berry (*Triphasia trifolia*, which produces two thorns per leaf axil) (Figures 6A–6I). We identified *Ti3* homologs in these species and found that their protein sequences share a high degree of similarity (over 96% identity) (Figures S6A and S6B). These homologs also exhibited preferential expression in thorns (Figures 6J–6L). RNA *in situ* hybridization confirmed this specific expression pattern, showing sustained *Ti3* homolog expression from the primordium stage through to pointed thorn development in Australian finger lime (Figure 6M). Notably, *Ti3* mRNA was detected in thorns of Chinese box orange and in both thorns of lime berry (Figures 6N and 6O). These results suggest that the *Ti3*-mediated genetic module is a conserved mechanism underlying thorn identity determination within Rutaceae.

DISCUSSION

In this study, we demonstrate a fundamental role for the SHI/STY family transcription factor Ti3 in terminating stem cell activity within the TM. We show that Ti3 represses the expression of *CsWUS*, a key marker of shoot meristem stem cell activity, through the timely activation of two functionally redundant *TCP* genes, *Ti1* and *Ti2*. Conversely, the PEBP family protein *CsCEN* spatially restricts thorn development by suppressing *Ti3* expression in the AM, thereby preserving its stem cell activity and indeterminate state. The consistent expression pattern of *Ti3* homologs across three Rutaceae species suggests that *Ti3* might have a conserved role in thorn development within this family. Together, our findings elucidate how stem cell activity is antagonistically regulated in two distinct meristems that occupy the same leaf axil in close proximity yet exhibit divergent developmental fates (Figure 7).

The *Ti3-Ti1/2-CsWUS* pathway promotes thorn identity

Timely negative feedback regulation is essential for determinate growth in shoot meristems.²⁹ Notably, *Ti3* expression is initiated at stage 4 and subsequently activates *Ti2* (stage 7) and *Ti1* (stage 8). Together, *Ti1* and *Ti2* terminate *CsWUS* expression by stage 8, ensuring the precise thorn formation. Disrupting this cascade—either by mutating *Ti3* alone or both *Ti1* and *Ti2*—converts thorns into branches. This mechanism parallels the termination of stem cell activity in the *Arabidopsis* floral meristem. There, the meristem identity regulator *LFY* activates

(B) Quantitative real-time PCR analysis of *Ti1*, *Ti2*, and *Ti3* expression in young shoots of WT and *ti3*. Error bars represent means \pm SD ($n = 3$ biological replicates). ** $p < 0.01$, *** $p < 0.001$ (Student's *t* test).

(C and D) Distribution of Ti3 DAP-seq peaks (C) and the most significant Ti3-binding motif (D).

(E and F) Browser view of Ti3 binding peaks at the *Ti1* (E) and *Ti2* (F) loci. Peak (1/2), T1-T3, and T3m/T2m (mutated *cis*-motifs) indicate promoter sequences tested in transcriptional activation assays. Magenta shading shows regions with CTAG motifs (5 in *proTi1P*, 2 in *proTi2P1*, and 6 in *proTi2P2*), whereas gray shading shows the same regions with all CTAG motifs mutated.

(G) Schematic of reporter and effector constructs.

(H–J) Ti3 activates the *Ti1* and *Ti2* promoters via CTAG motifs. Transcriptional activation assays using *Ti1* (H) or *Ti2* (I with Peak1, J with Peak2) promoter fragments or mutant reporters. Locations of *Ti1* or *Ti2* promoter fragments are shown in (E) and (F), respectively. Mutation in CTAG motifs (T3m in H, T2m in I and J) abolishes activation. Error bars represent means \pm SD ($n = 4$ biological replicates), * $p < 0.05$, ** $p < 0.01$, and *** $p < 0.001$ (Student's *t* test).

(K) DNA probes used in EMSAs: labeled WT probes (Ti1P, Ti2P1, and Ti2P2 from Ti3 binding regions in *proTi1* and *proTi2*), unlabeled competitor probes (cTi1P, cTi2P1, and cTi2P2), and labeled mutated probes (mTi1P, mTi2P1, and mTi2P2) with mutated CTAG motifs.

(L) EMSA showing specific binding of recombinant GST-Ti3 to WT, but not mutated, probes. Competition with the unlabeled probe (10 \times) confirms specificity. See also Figures S3–S5 and S7 and Data S3–S5.

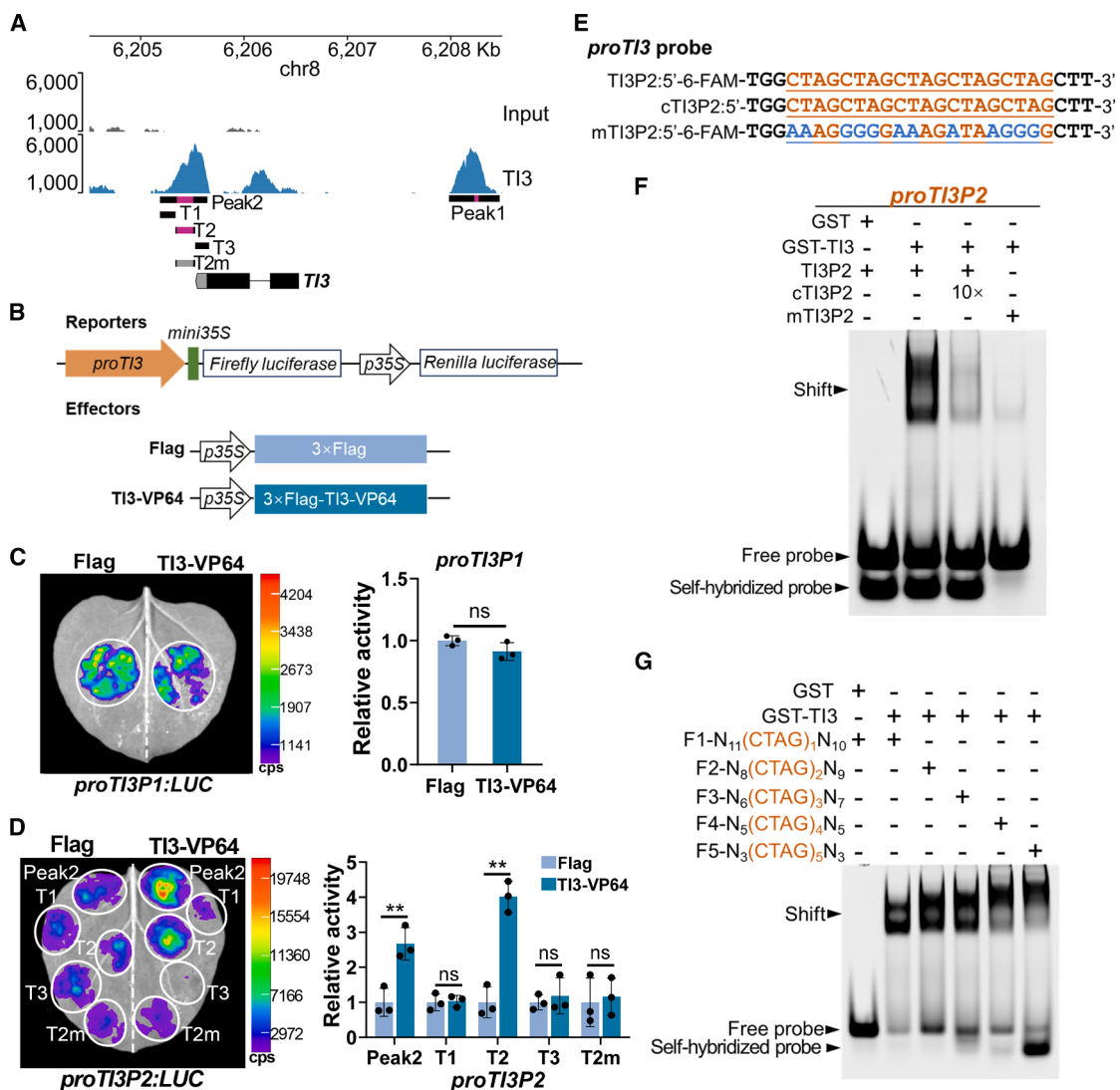


Figure 5. TI3 enables self-activation by binding to its own 3' UTR

(A) Browser view of TI3-binding peaks at the *T13* locus. Peak 1, Peak 2, T1 to T3, and T2m (mutated *cis*-motifs) represent promoter sequences tested in transcriptional activation assays. Magenta shading indicates regions containing the CTAG motifs (1 in Peak1, 5 in Peak2), and gray shading indicates the same regions with all CTAG motifs mutated.

(B–D) TI3 activates its own promoter.

(B) Schematic of the reporter and effector constructs.

(C and D) Transcriptional activation assays show TI3-VP64 activity on different *T13* promoter fragments (C, Peak1, *proT13P1*; D, Peak2, *proT13P2*). Error bars represent means \pm SD ($n = 3$ biological replicates), ** $p < 0.01$ (Student's *t* test).

(E) Probes used for EMSA: TI3P2 (from Peak2 of *proT13*), unlabeled competitor probe (cT13P2), and mutant probe (mT13P2) with core CTAG motifs mutated.

(F) EMSA shows specific binding of GST-TI3 to the WT probe, which is competed away by the unlabeled probe (10 \times) and abolished by CTAG mutation. Self-hybridization probe was formed after annealing due to five palindromic CTAG repeats.

(G) EMSA using recombinant GST-TI3 and a series of 25/26-bp probes (F1–F5) containing 1 to 5 copies of the CTAG motif. Probes were designed based on the promoter sequences of *T13* (F1, F4, F5) and *T11* (F2, F3).

See also [Data S4](#).

AGAMOUS (AG), which represses *WUS* to terminate stem cell activity and promote proper floral organ patterning.^{5,30,31} Notably, AG expression begins at stage 3, and it activates KNUCKLES (KNU) at stage 6.^{32,33} KNU recruits histone deacetylase complexes to epigenetically silence *WUS* expression.³⁴ Recent studies also indicate that KNU can regulate stem cell

activity via CLAVATA genes, which form a negative regulatory loop with *WUS*.³⁵ However, we were unable to detect CsAG expression during thorn development.⁷ Thus, although both the TM and floral meristem are determinate shoot meristems, they appear to regulate *WUS* expression through distinct pathways.

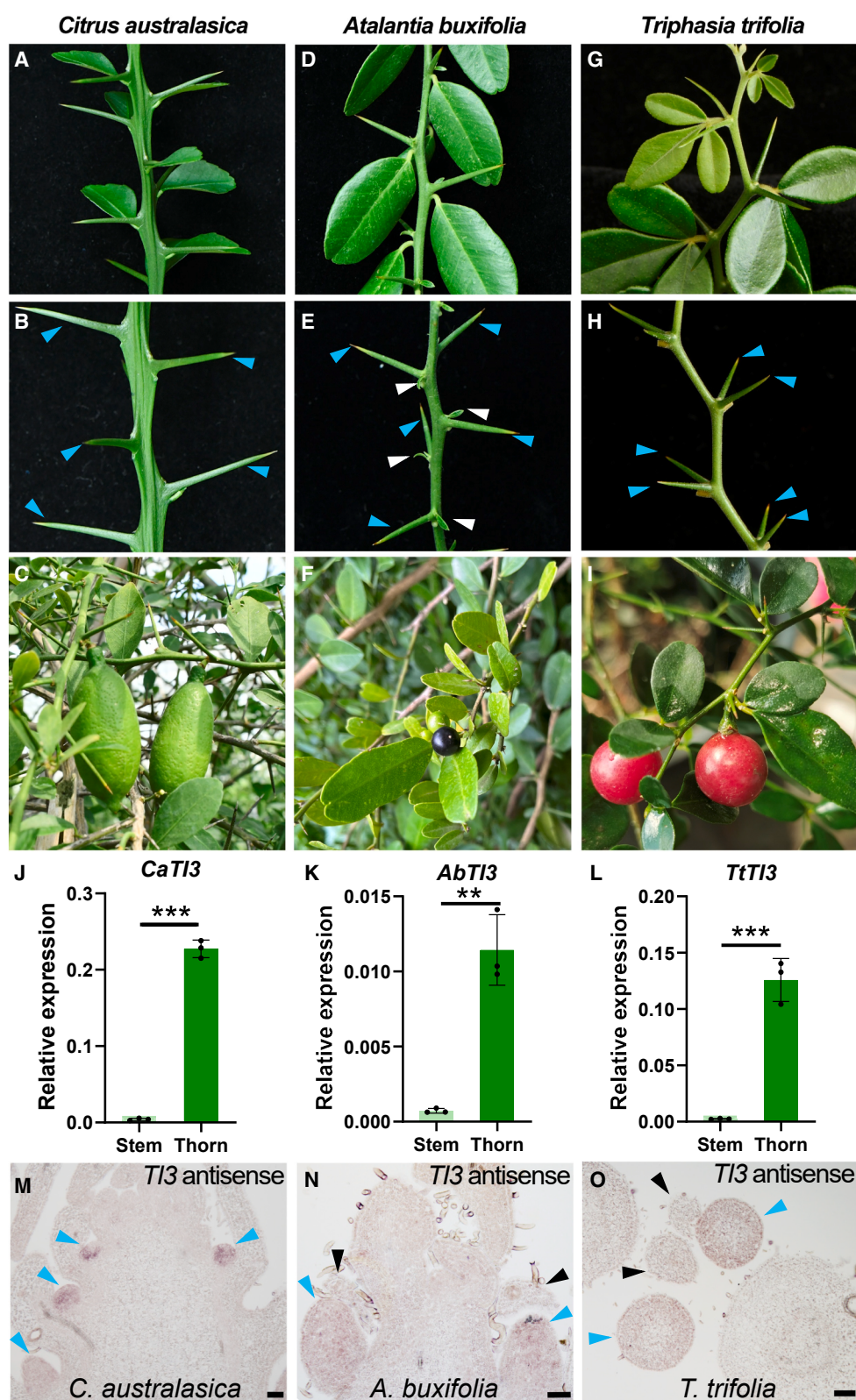
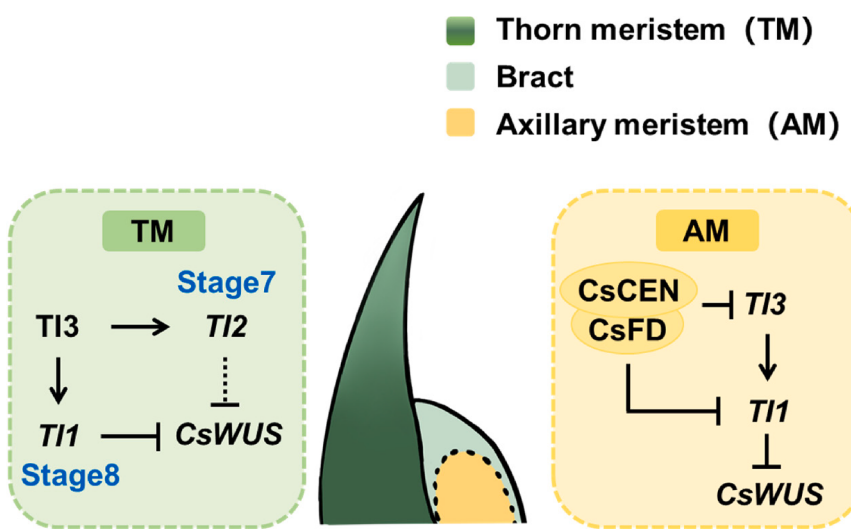


Figure 6. Thorn-specific expression of *T3* homologs in three Rutaceae species

(A–I) Phenotypes of Australian finger lime (*Citrus australasica*) (A–C), Chinese box orange (*Atalantia buxifolia*) (D–F), and lime berry (*Triphasia trifolia*) (G–I). Blue, thorns; white, bracts.

(legend continued on next page)



CsCEN represses *Tl3* to maintain AM stem cell activity

Citrus provides a great model system for studying vegetative shoot meristem determinacy due to its clear spatial distinction between indeterminate AMs and determinate TMs. We previously identified *CsCEN* as a regulator of AM identity via its repression of *Tl1* promoter activity.⁸ Here we demonstrate that *CsCEN* also suppresses *Tl3* promoter activity, preventing thorn development within its expression domain. In the *cscen* mutant background, mutations in *Tl3* fully convert ectopic thorn growth into branches. This differential expression acts as a binary switch: where *CsCEN* is absent, *Tl3* imposes determinacy, and where present, *CsCEN* represses *Tl3*, enabling indeterminacy. The antagonistic interaction between *CsCEN* and *Tl3* parallels the relationship between *TFL1* and *LFY* in inflorescence meristem and floral meristem, respectively.^{36,37} A key difference, however, is that the floral meristem is derived from the inflorescence meristem, whereas AM and TM arise simultaneously and are both axillary in origin.

Tl3 binds CTAG core motif to regulate downstream genes

Tl3 is an ortholog of *Arabidopsis* *SRS3*, whose functions remain poorly characterized. We show that *Tl3* binds to CTAG motifs arranged in tandem repeats within the promoters of *Tl1* and *Tl2*. A similar “CTAGCTAG” motif was detected in SELEX DNA-binding assays of *AtSTY1*.³⁸ This motif differs from the previously reported T/GCTCTAC motif and has been largely overlooked.¹² Interestingly, in rice, *OsSHI1* interacts with *IPA1* to repress its activation of *OsTB1* (a homolog of *Citrus Tl1*) and can bind the T/GCTCTAC motif in the *OsTB1* promoter.²² The activation or repression of homologous genes across species may reflect context-dependent interactions with distinct protein partners.

Tl3 appears to function within auxin signaling. Asymmetric auxin distribution around developing leaf primordia may contribute to

Figure 7. A model of *Tl3*-mediated specification of AM fate

In the thorn developmental pathway (left), *Tl3* expression is initiated at stage 4 and subsequently activates *Tl2* (stage 7) and *Tl1* (stage 8) to promote determinacy. *Tl1* and *Tl2* together terminate *CsWUS* expression at stage 8 thorn primordium. In the AM maintenance pathway (right), the *CsCEN*-*CsFD* complex represses *Tl3* and *Tl1*, thereby sustaining *CsWUS* expression and meristem indeterminacy.

meristem identity divergence.³⁹ Members of the SHI/STY family participate in auxin homeostasis. For instance, *AtSTY1* promotes auxin biosynthesis by activating *YUC2* and *YUC8*.^{12–14,40} In *tl3* mutants, two auxin biosynthetic genes, *CsYUC2*

and *CsYUC8*, are downregulated (Data S3; Figures S7A and S7B). *Tl3*-binding peaks containing core CTAG motifs were identified in the promoters of both *CsYUC* genes (Figures S7C and S7D), suggesting they are direct targets of *Tl3*. The roles of these *CsYUC* genes in thorn development require further investigation.

Thorns are a hallmark of juvenility in citrus trees. As trees mature, particularly mandarins, thorn production declines markedly on most branches. A notable exception is the “water sprout”—a vigorous, seedling-like shoot that can emerge after environmental stress, such as overwatering, and retains strong thorn development. This correlation between a rejuvenated growth habit and thorn recurrence suggests that the expression of thorn identity genes is likely regulated by developmental and environmental cues, potentially through epigenetic mechanisms, a hypothesis that warrants further investigation.

While thorns serve as a primary defense against herbivores in nature, they present substantial challenges in agriculture. Thorns complicate cultivation, increase labor costs for pruning and harvesting, and can damage both fruits and workers. This is particularly problematic in economically important varieties such as the rootstocks *P. trifoliata* and Carrizo citrange and in the huanglongbing-tolerant Australian finger lime. The conserved expression of *Tl3* homologs across Rutaceae points to its role in a core regulatory module for thorn formation. Thus, the *Tl3* pathway likely represents a conserved genetic mechanism controlling thorn development, enabling broad modification through targeted breeding.

RESOURCE AVAILABILITY

Lead contact

Further information and requests for resources and reagents should be directed to and will be fulfilled by the lead contact, Fei Zhang (feizhang@mail.hzau.edu.cn).

(J–L) Quantitative real-time PCR analysis of *CaTl3*, *AbTl2*, and *TtTl3* expression in young stems and thorns. Error bars represent means \pm SD ($n = 3$ biological replicates). $^{*}p < 0.01$, $^{**}p < 0.001$ (Student's *t* test).

(M–O) RNA *in situ* expression of the *Tl3* homologs in Australian finger lime (M), Chinese box orange (N), and lime berry (O). Blue, thorns; black, bracts. Scale bars, 50 μ m.

See also Figure S6.

Materials availability

Requests for materials should be addressed to the [lead contact](#).

Data and code availability

- The RNA-seq and DAP-seq data have been deposited in the NGDC database with accession number CRA030186 (<https://ngdc.cncb.ac.cn/gsa/browse/CRA030186>).
- This paper does not report original code.
- Any additional information in this paper is available from the [lead contact](#) upon request.

ACKNOWLEDGMENTS

We thank Zongzhou Xie for providing plant materials, Dr. Miao Sun for help with phylogenetic analysis, and members of the Irish lab at Yale University for comments on the manuscript. This work was supported by the National Natural Science Foundation of China (32172541 and 32425048).

AUTHOR CONTRIBUTIONS

Q.Z. and S.Z. performed experiments. V.F.I. and F.Z. supervised the project. Q.Z. and F.Z. conceived the project and wrote the manuscript. All the authors reviewed and approved the final version of the manuscript.

DECLARATION OF INTERESTS

A patent has been filed by the Huazhong Agricultural University (China patents: 202511644823.2).

STAR★METHODS

Detailed methods are provided in the online version of this paper and include the following:

- [KEY RESOURCES TABLE](#)
- [EXPERIMENTAL MODEL AND STUDY PARTICIPANT DETAILS](#)
- [METHOD DETAILS](#)
 - Plasmid constructions and plant transformation
 - Phylogenetic analysis
 - Subcellular localization
 - Multiple sequence alignment of TI3 homologs
 - Dual-luciferase assays
 - DNA affinity purification sequencing (DAP-seq)
 - Transcriptome analysis
 - Electrophoretic mobility-shift assays (EMSA)
 - Quantitative real-time PCR (QRT-PCR)
 - RNA *in situ* hybridization
 - Scanning electron microscopy (SEM)
- [QUANTIFICATION AND STATISTICAL ANALYSIS](#)

SUPPLEMENTAL INFORMATION

Supplemental information can be found online at <https://doi.org/10.1016/j.cub.2026.01.002>.

Received: September 24, 2025

Revised: November 29, 2025

Accepted: January 5, 2026

REFERENCES

1. Sluis, A., and Hake, S. (2015). Organogenesis in plants: initiation and elaboration of leaves. *Trends Genet.* 31, 300–306. <https://doi.org/10.1016/j.tig.2015.04.004>.
2. Arnoux-Courseaux, M., and Coudert, Y. (2024). Re-examining meristems through the lens of evo-devo. *Trends Plant Sci.* 29, 413–427. <https://doi.org/10.1016/j.tplants.2023.11.003>.
3. Greb, T., and Lohmann, J.U. (2016). Plant stem cells. *Curr. Biol.* 26, R816–R821. <https://doi.org/10.1016/j.cub.2016.07.070>.
4. Alvarez, J.P., Furumizu, C., Efroni, I., Eshed, Y., and Bowman, J.L. (2016). Active suppression of a leaf meristem orchestrates determinate leaf growth. *eLife* 5, e15023. <https://doi.org/10.7554/eLife.15023>.
5. Lenhard, M., Bohnert, A., Jürgens, G., and Lax, T. (2001). Termination of stem cell maintenance in *Arabidopsis* floral meristems by interactions between *WUSCHEL* and *AGAMOUS*. *Cell* 105, 805–814. [https://doi.org/10.1016/S0092-8674\(01\)00390-7](https://doi.org/10.1016/S0092-8674(01)00390-7).
6. Steeves, T.A., and Sussex, I.M. (1989). Patterns in Plant Development, Second Edition (Cambridge University Press). <https://doi.org/10.1017/CBO9780511626227>.
7. Zhang, F., Rossignol, P., Huang, T., Wang, Y., May, A., Dupont, C., Orbovic, V., and Irish, V.F. (2020). Reprogramming of stem cell activity to convert thorns into branches. *Curr. Biol.* 30, 2951–2961.e5. <https://doi.org/10.1016/j.cub.2020.05.068>.
8. Zhang, F., Wang, Y., and Irish, V.F. (2021). *CENTRORADIALIS* maintains shoot meristem indeterminacy by antagonizing *THORN IDENTITY1* in *Citrus*. *Curr. Biol.* 31, 2237–2242.e4. <https://doi.org/10.1016/j.cub.2021.02.051>.
9. Airoldi, C.A., and Glover, B.J. (2020). Evo-Devo: tinkering with the stem cell niche to produce thorns. *Curr. Biol.* 30, R873–R875. <https://doi.org/10.1016/j.cub.2020.06.019>.
10. Kuusk, S., Sohlberg, J.J., Magnus Eklund, D., and Sundberg, E. (2006). Functionally redundant *SHI* family genes regulate *Arabidopsis* gynoecium development in a dose-dependent manner. *Plant J.* 47, 99–111. <https://doi.org/10.1111/j.1365-313X.2006.02774.x>.
11. Eklund, D.M., Thelander, M., Landberg, K., Ståldal, V., Nilsson, A., Johansson, M., Valsecchi, I., Pederson, E.R.A., Kowalczyk, M., Ljung, K., et al. (2010). Homologues of the *Arabidopsis thaliana* *SHI/STY/LRP1* genes control auxin biosynthesis and affect growth and development in the moss *Physcomitrella patens*. *Development* 137, 1275–1284. <https://doi.org/10.1242/dev.039594>.
12. Eklund, D.M., Ståldal, V., Valsecchi, I., Cierlik, I., Eriksson, C., Hiratsu, K., Ohme-Takagi, M., Sundström, J.F., Thelander, M., Ezcurra, I., et al. (2010). The *Arabidopsis thaliana* STYLISH1 protein acts as a transcriptional activator regulating auxin biosynthesis. *Plant Cell* 22, 349–363. <https://doi.org/10.1105/tpc.108.064816>.
13. Ståldal, V., Cierlik, I., Chen, S., Landberg, K., Baylis, T., Myrenås, M., Sundström, J.F., Eklund, D.M., Ljung, K., and Sundberg, E. (2012). The *Arabidopsis thaliana* transcriptional activator STYLISH1 regulates genes affecting stamen development, cell expansion and timing of flowering. *Plant Mol. Biol.* 78, 545–559. <https://doi.org/10.1007/s11103-012-9888-z>.
14. Sohlberg, J.J., Myrenås, M., Kuusk, S., Lagercrantz, U., Kowalczyk, M., Sandberg, G., and Sundberg, E. (2006). *STY1* regulates auxin homeostasis and affects apical-basal patterning of the *Arabidopsis* gynoecium. *Plant J.* 47, 112–123. <https://doi.org/10.1111/j.1365-313X.2006.02775.x>.
15. Estornell, L.H., Landberg, K., Cierlik, I., and Sundberg, E. (2018). *SHI/STY* genes affect pre- and post-meiotic anther processes in auxin sensing domains in *Arabidopsis*. *Front. Plant Sci.* 9, 1–16. <https://doi.org/10.3389/fpls.2018.00150>.
16. Landberg, K., Pederson, E.R.A., Viaene, T., Bozorg, B., Friml, J., Jönsson, H., Thelander, M., and Sundberg, E. (2013). The moss *physcomitrella patens* reproductive organ development is highly organized, affected by the two *SHI/STY* genes and by the level of active auxin in the *SHI/STY* expression domain. *Plant Physiol.* 162, 1406–1419. <https://doi.org/10.1104/pp.113.214023>.
17. Yuan, T.T., Xu, H.H., Zhang, Q., Zhang, L.Y., and Lu, Y.T. (2018). The COP1 target SHI-RELATED SEQUENCE5 directly activates photomorphogenesis-promoting genes. *Plant Cell* 30, 2368–2382. <https://doi.org/10.1105/tpc.18.00455>.

18. Yuan, T.T., Xu, H.H., Li, J., and Lu, Y.T. (2020). Auxin abolishes *SHI-RELATED SEQUENCE5*-mediated inhibition of lateral root development in *Arabidopsis*. *New Phytol.* 225, 297–309. <https://doi.org/10.1111/nph.16115>.
19. Shrestha, A., Zhong, S., Therrien, J., Huebert, T., Sato, S., Mun, T., Andersen, S.U., Stougaard, J., Lepage, A., Niebel, A., et al. (2021). *Lotus japonicus* Nuclear Factor YA1, a nodule emergence stage-specific regulator of auxin signalling. *New Phytol.* 229, 1535–1552. <https://doi.org/10.1111/nph.16950>.
20. Zawaski, C., Kadmiel, M., Ma, C., Gai, Y., Jiang, X., Strauss, S.H., and Busov, V.B. (2011). SHORT INTERNODES-like genes regulate shoot growth and xylem proliferation in *Populus*. *New Phytol.* 191, 678–691. <https://doi.org/10.1111/j.1469-8137.2011.03742.x>.
21. Min, Y., Bunn, J.I., and Kramer, E.M. (2019). Homologs of the *STYLISH* gene family control nectary development in *Aquilegia*. *New Phytol.* 221, 1090–1100. <https://doi.org/10.1111/nph.15406>.
22. Duan, E., Wang, Y., Li, X., Lin, Q., Zhang, T., Wang, Y., Zhou, C., Zhang, H., Jiang, L., Wang, J., et al. (2019). OsSHI1 regulates plant architecture through modulating the transcriptional activity of IPA1 in rice. *Plant Cell* 31, 1026–1042. <https://doi.org/10.1105/tpc.19.00023>.
23. Youssef, H.M., Eggert, K., Koppolu, R., Alqudah, A.M., Poursarebani, N., Fazeli, A., Sakuma, S., Tagiri, A., Rutten, T., Govind, G., et al. (2017). VRS2 regulates hormone-mediated inflorescence patterning in barley. *Nat. Genet.* 49, 157–161. <https://doi.org/10.1038/ng.3717>.
24. Ren, J., Duan, Y., Li, R., Zhang, X., Shi, Y., Zhou, S., Xie, K., Wu, X., Irish, V.F., Deng, X., et al. (2025). Transcriptional regulation of thorn tip sclerification in plants. *Proc. Natl. Acad. Sci. USA* 122, e2510775122. <https://doi.org/10.1073/pnas.2510775122>.
25. Beerli, R.R., Segal, D.J., Dreier, B., and Barbas, C.F. (1998). Toward controlling gene expression at will: specific regulation of the *erbB-2/HER-2* promoter by using polydactyl zinc finger proteins constructed from modular building blocks. *Proc. Natl. Acad. Sci. USA* 95, 14628–14633. <https://doi.org/10.1073/pnas.95.25.14628>.
26. Hiratsuka, K., Matsui, K., Koyama, T., and Ohme-Takagi, M. (2003). Dominant repression of target genes by chimeric repressors that include the EAR motif, a repression domain, in *Arabidopsis*. *Plant J.* 34, 733–739. <https://doi.org/10.1046/j.1365-313X.2003.01759.x>.
27. Aguilar-Martínez, J.A., Poza-Carrión, C., and Cubas, P. (2007). *Arabidopsis* BRANCHED1 acts as an integrator of branching signals within axillary buds. *Plant Cell* 19, 458–472. <https://doi.org/10.1105/tpc.106.048934>.
28. González-Grandío, E., Pajoro, A., Franco-Zorrilla, J.M., Tarancón, C., Immink, R.G.H., and Cubas, P. (2016). Abscisic acid signaling is controlled by a BRANCHED1/HD-ZIP I cascade in *Arabidopsis* axillary buds. *Proc. Natl. Acad. Sci. USA* 114, E245–E254. <https://doi.org/10.1073/pnas.1613199114>.
29. Coen, E., and Prusinkiewicz, P. (2024). Developmental timing in plants. *Nat. Commun.* 15, 2674. <https://doi.org/10.1038/s41467-024-46941-1>.
30. Liu, X., Kim, Y.J., Müller, R., Yumul, R.E., Liu, C., Pan, Y., Cao, X., Goodrich, J., and Chen, X. (2011). AGAMOUS terminates floral stem cell maintenance in *Arabidopsis* by directly repressing *WUSCHEL* through recruitment of Polycomb group proteins. *Plant Cell* 23, 3654–3670. <https://doi.org/10.1105/tpc.111.091538>.
31. Lohmann, J.U., Hong, R.L., Hobe, M., Busch, M.A., Parcy, F., Simon, R., and Weigel, D. (2001). A molecular link between stem cell regulation and floral patterning in *Arabidopsis*. *Cell* 105, 793–803. [https://doi.org/10.1016/S0092-8674\(01\)00384-1](https://doi.org/10.1016/S0092-8674(01)00384-1).
32. Sun, B., Xu, Y., Ng, K.H., and Ito, T. (2009). A timing mechanism for stem cell maintenance and differentiation in the *Arabidopsis* floral meristem. *Genes Dev.* 23, 1791–1804. <https://doi.org/10.1101/gad.1800409>.
33. Sun, B., Looi, L.S., Guo, S., He, Z., Gan, E.S., Huang, J., Xu, Y., Wee, W.Y., and Ito, T. (2014). Timing mechanism dependent on cell division is invoked by Polycomb eviction in plant stem cells. *Science* 343, 1248559. <https://doi.org/10.1126/science.1248559>.
34. Bollier, N., Sicard, A., Leblond, J., Latrasse, D., Gonzalez, N., Gévaudant, F., Benhamed, M., Raynaud, C., Lenhard, M., Chevalier, C., et al. (2018). At-MINI ZINC FINGER2 and SI-INHIBITOR of MERISTEM ACTIVITY, a conserved missing link in the regulation of floral meristem termination in *Arabidopsis* and tomato. *Plant Cell* 30, 83–100. <https://doi.org/10.1105/tpc.17.00653>.
35. Shang, E., Wang, X., Li, T., Guo, F., Ito, T., and Sun, B. (2021). Robust control of floral meristem determinacy by position-specific multifunctions of KNUCKLES. *Proc. Natl. Acad. Sci. USA* 118, e2102826118. <https://doi.org/10.1073/pnas.2102826118>.
36. Shannon, S., and Meeks-Wagner, D.R. (1993). Genetic interactions that regulate inflorescence development in *Arabidopsis*. *Plant Cell* 5, 639–655. <https://doi.org/10.1105/tpc.5.6.639>.
37. Périlleux, C., Bouché, F., Randoux, M., and Orman-Ligeza, B. (2019). Turning meristems into fortresses. *Trends Plant Sci.* 24, 431–442. <https://doi.org/10.1016/j.tplants.2019.02.004>.
38. Franco-Zorrilla, J.M., López-Vidriero, I., Carrasco, J.L., Godoy, M., Vera, P., and Solano, R. (2014). DNA-binding specificities of plant transcription factors and their potential to define target genes. *Proc. Natl. Acad. Sci. USA* 111, 2367–2372. <https://doi.org/10.1073/pnas.1316278111>.
39. Leichty, A.R., and Sinha, N.R. (2021). Plant development: how competing modes of growth coexist in close proximity. *Curr. Biol.* 31, R472–R474. <https://doi.org/10.1016/j.cub.2021.03.073>.
40. Baylis, T., Cierlik, I., Sundberg, E., and Mattsson, J. (2013). SHORT INTERNODES/STYLISH genes, regulators of auxin biosynthesis, are involved in leaf vein development in *Arabidopsis thaliana*. *New Phytol.* 197, 737–750. <https://doi.org/10.1111/nph.12084>.
41. Zhang, F., LeBlanc, C., Irish, V.F., and Jacob, Y. (2017). Rapid and efficient CRISPR/Cas9 gene editing in *Citrus* using the YAO promoter. *Plant Cell Rep.* 36, 1883–1887. <https://doi.org/10.1007/S00299-017-2202-4>.
42. Earley, K.W., Haag, J.R., Pontes, O., Opper, K., Juehne, T., Song, K., and Pikaard, C.S. (2006). Gateway-compatible vectors for plant functional genomics and proteomics. *Plant J.* 45, 616–629. <https://doi.org/10.1111/j.1365-313X.2005.02617.x>.
43. Hellens, R.P., Allan, A.C., Friel, E.N., Bolitho, K., Grafton, K., Templeton, M.D., Karunaratnam, S., Gleave, A.P., and Laing, W.A. (2005). Transient expression vectors for functional genomics, quantification of promoter activity and RNA silencing in plants. *Plant Methods* 1, 13. <https://doi.org/10.1186/1746-4811-1-13>.
44. Kumar, S., Stecher, G., and Tamura, K. (2016). MEGA7: molecular evolutionary genetics analysis version 7.0 for bigger datasets. *Mol. Biol. Evol.* 33, 1870–1874. <https://doi.org/10.1093/MOLBEV/MSW054>.
45. Edgar, R.C. (2004). MUSCLE: a multiple sequence alignment method with reduced time and space complexity. *BMC Bioinform.* 5, 113. <https://doi.org/10.1186/1471-2105-5-113>.
46. Minh, B.Q., Schmidt, H.A., Chernomor, O., Schrempf, D., Woodhams, M.D., von Haeseler, A. Von, and Lanfear, R. (2020). IQ-TREE 2: new models and efficient methods for phylogenetic inference in the genomic era. *Mol. Biol. Evol.* 37, 1530–1534. <https://doi.org/10.1093/molbev/msaa015>.
47. Yu, G. (2020). Using ggtree to visualize data on tree-like structures. *Curr. Protoc. Bioinform.* 69, e96. <https://doi.org/10.1002/cpb1.96>.
48. Wheeler, T.J., and Eddy, S.R. (2013). nhmm: DNA homology search with profile HMMs. *Bioinformatics* 29, 2487–2489. <https://doi.org/10.1093/bioinformatics/btt403>.
49. Langmead, B., and Salzberg, S.L. (2012). Fast gapped-read alignment with Bowtie 2. *Nat. Methods* 9, 357–359. <https://doi.org/10.1038/nmeth.1923>.
50. Zhang, Y., Liu, T., Meyer, C.A., Eeckhoute, J., Johnson, D.S., Bernstein, B.E., Nusbaum, C., Myers, R.M., Brown, M., Li, W., et al. (2008). Model-based analysis of ChIP-seq (MACS). *Genome Biol.* 9, R137. <https://doi.org/10.1186/gb-2008-9-9-r137>.
51. Heinz, S., Benner, C., Spann, N., Bertolino, E., Lin, Y.C., Laslo, P., Cheng, J.X., Murre, C., Singh, H., and Glass, C.K. (2010). Simple combinations of

- lineage-determining transcription factors prime *cis*-regulatory elements required for macrophage and B cell identities. *Mol. Cell* 38, 576–589. <https://doi.org/10.1016/j.molcel.2010.05.004>.
52. Yu, G., Wang, L.G., and He, Q.Y. (2015). ChIPseeker: an R/Bioconductor package for ChIP peak annotation, comparison and visualization. *Bioinformatics* 31, 2382–2383. <https://doi.org/10.1093/bioinformatics/btv145>.
53. Chen, S., Zhou, Y., Chen, Y., and Gu, J. (2018). Fastp: an ultra-fast all-in-one FASTQ preprocessor. *Bioinformatics* 34, i884–i890. <https://doi.org/10.1093/bioinformatics/bty560>.
54. Pertea, M., Kim, D., Pertea, G.M., Leek, J.T., and Salzberg, S.L. (2016). Transcript-level expression analysis of RNA-seq experiments with HISAT, StringTie and Ballgown. *Nat. Protoc.* 11, 1650–1667. <https://doi.org/10.1038/nprot.2016.095>.
55. Danecek, P., Bonfield, J.K., Liddle, J., Marshall, J., Ohan, V., Pollard, M.O., Whittham, A., Keane, T., McCarthy, S.A., Davies, R.M., et al. (2021). Twelve years of SAMtools and BCFtools. *GigaScience* 10, giab008. <https://doi.org/10.1093/gigascience/giab008>.
56. Love, M.I., Huber, W., and Anders, S. (2014). Moderated estimation of fold change and dispersion for RNA-seq data with DESeq2. *Genome Biol.* 15, 550. <https://doi.org/10.1186/s13059-014-0550-8>.
57. Khadgi, A., Sagawa, C.H.D., Vernon, C., Mermaz, B., and Irish, V.F. (2024). Optimization of *in planta* methodology for genome editing and transformation in *Citrus*. *Front. Plant Sci.* 15, 1438031. <https://doi.org/10.3389/fpls.2024.1438031>.
58. Liu, Q., Wang, C., Jiao, X., Zhang, H., Song, L., Li, Y., Gao, C., and Wang, K. (2019). Hi-TOM: a platform for high-throughput tracking of mutations induced by CRISPR/Cas systems. *Sci. China Life Sci.* 62, 1–7. <https://doi.org/10.1007/s11427-018-9402-9>.
59. Wang, H., Ren, J., Zhou, S., Duan, Y., Zhu, C., Chen, C., Liu, Z., Zheng, Q., Xiang, S., Xie, Z., et al. (2024). Molecular regulation of oil gland development and biosynthesis of essential oils in *Citrus* spp. *Science* 383, 659–666. <https://doi.org/10.1126/science.adl2953>.
60. Carles, C.C., Ha, C.M., Jun, J.H., Fiume, E., and Fletcher, J.C. (2010). Analyzing shoot apical meristem development. *Methods Mol. Biol.* 655, 105–129. https://doi.org/10.1007/978-1-60761-765-5_8.

STAR★METHODS

KEY RESOURCES TABLE

REAGENT or RESOURCE	SOURCE	IDENTIFIER
Bacterial and virus strains		
<i>Agrobacterium tumefaciens</i> strain EHA105	Weidibio	Cat# AC1010
<i>Agrobacterium tumefaciens</i> strain GV3101	Weidibio	Cat# AC1001
<i>Escherichia coli</i> strain DH5 α	Weidibio	Cat# DL1001
Recombinant protein expression strain Rosetta (DE3)	Weidibio	Cat# EC1010
Chemicals, peptides, and recombinant proteins		
Murashige & Skoog Basal Medium with Vitamins	Phyto-tech	Cat# M519
Sucrose	Sigma-Aldrich	Cat# V900116
6-Benzylaminopurine	Sigma-Aldrich	Cat# B3408
1-Naphthaleneacetic acid	Sigma-Aldrich	Cat# N0640
Critical commercial assays		
pTOPO-Blunt Simple Cloning Kit	Aidlab	Cat# CV1701
Dual-luciferase Reporter Assay System	Promega	Cat# E1910
DIG RNA Labeling Kit (SP6/T7)	Roche	Cat# 11175025910
Gateway BP Clonase II enzyme mix	Invitrogen	Cat# 11789020
Gateway LR Clonase II enzyme mix	Invitrogen	Cat# 11791100
HiPure HP Plant RNA Mini Kit	Magen	Cat# R4165-02
QIAquick PCR Purification Kit	QIAGEN	Cat# 28104
QIAGEN Plasmid Plus Midi Kit	QIAGEN	Cat# 28181
ClonExpress II One Step Cloning Kit	Vazyme	Cat# C112-01
HiScript III RT SuperMix for qPCR	Vazyme	Cat# R323-01
Hieff qPCR SYBR Green Master Mix	YEASEN	Cat# 11201ES08
T4 DNA Ligase	NEB	Cat# M0202S
<i>Bsa</i> I-HF	NEB	Cat# R3535
<i>Bbs</i> I-HF	NEB	Cat# R3539
<i>Bam</i> H I-HF	NEB	Cat# R3136
<i>Kpn</i> I-HF	NEB	Cat# R3142
Deposited data		
Raw RNA-seq and DAP-seq data	This study	Accession NO. CRA030186 in NGDC database (https://ngdc.cncb.ac.cn/gsa/browse/CRA030186)
Citrus Genome Assembly and Annotation	<i>Citrus sinensis</i> v2.0	https://http://citrus.hzau.edu.cn/
Plant Transcription Factor Database	PlantTFdb	http://planttfdb.cbi.pku.edu.cn/
<i>Arabidopsis</i> genome	TAIR10	https://www.arabidopsis.org/
Experimental models: Organisms/strains		
Carrizo citrange	Huazhong Agricultural University	N/A
Oligonucleotides		
See Data S6	N/A	N/A
Recombinant DNA		
pDONR207	Thermo Fisher	pDONR207
pCambia1300	Thermo Fisher	K240020
pTOPO-Blunt Simple	Aidlab	Cat# CV1701
proYAO-hspCas9-NOS vector	Zhang et al. ⁴¹	N/A
AtU6-26-sgRNA-SK vector	Zhang et al. ⁴¹	N/A

(Continued on next page)

Continued

REAGENT or RESOURCE	SOURCE	IDENTIFIER
pEarleyGate 104	Earley et al. ⁴²	N/A
pGREEN0800II-LUC	Hellens et al. ⁴³	N/A
Software and algorithms		
MEGA7	Kumar et al. ⁴⁴	https://www.megasoftware.net/
MUSCLE	Edgar ⁴⁵	http://www.drive5.com/muscle
IQTREE	Minh et al. ⁴⁶	https://github.com/iqtree/iqtree2
Ggtree	Yu ⁴⁷	https://guangchuangyu.github.io/software/ggtree/
Hmmsearch	Wheeler and Eddy ⁴⁸	http://hmmer.org/
Bowtie2	Langmead and Salzberg ⁴⁹	https://github.com/BenLangmead/bowtie2
MACS2	Zhang et al. ⁵⁰	https://hbctraining.github.io/Intro-to-ChIPseq/lessons/05_peak_calling_macs.html
HOMER	Heinz et al. ⁵¹	http://homer.ucsd.edu/homer/
ChIPseeker	Yu et al. ⁵²	https://bioconductor.org/packages/release/bioc/html/ChIPseeker.html
Fastp	Chen et al. ⁵³	https://github.com/OpenGene/fastp
HISAT2	Pertea et al. ⁵⁴	https://daehwankimlab.github.io/hisat2/
SAMtools	Danecek et al. ⁵⁵	https://github.com/samtools/samtools
DESeq2	Love et al. ⁵⁶	https://bioconductor.org/packages/devel/bioc/vignettes/DESeq2/inst/doc/DESeq2.html

EXPERIMENTAL MODEL AND STUDY PARTICIPANT DETAILS

Carrizo citrange (*Citrus sinensis* 'Washington' sweet orange \times *Poncirus trifoliata*) was used as the experimental model. Carrizo citrange is a common rootstock worldwide. It is ideal for thorn development research due to stable thorn outgrowth at each leaf axil and high efficiency in genome editing. Carrizo citrange, *P. trifoliata*, and *Triphasia trifolia* (lime berry) were grown under long-day conditions (22°C, 16 h light/8 h dark).

Australian finger lime (*Citrus australasica*) and Chinese box orange (*Atalantia buxifolia*) were grown at the National Citrus Breeding Center, Huazhong Agricultural University, Wuhan, China.

METHOD DETAILS

Plasmid constructions and plant transformation

CRISPR-Cas9 genome editing constructs were produced as previously described.⁴¹ The primers for generating gRNAs of *Tl3*, *Tl1*, *Tl2*, *CsCEN*, and candidate transcription factor genes are listed in [Data S6](#).

For Carrizo citrange transformation, all binary constructs were introduced into *Agrobacterium tumefaciens* strain EHA105. *In planta* transformation of Carrizo citrange was employed, following a previously described methodology⁵⁷ with some modifications. Primers used for genotyping are listed in [Data S6](#), the induced mutations by CRISPR-Cas9 were tracked by NGS-based Hi-TOM sequencing platform.⁵⁸ Genotyping results are shown in [Data S2](#).

Phylogenetic analysis

The SHI/STY family members of *Arabidopsis thaliana* were downloaded from TAIR website (<http://www.arabidopsis.org/>). Homologs in *Lotus japonicus*, *Populus trichocarpa*, *Aquilegia coerulea*, *Oryza sativa*, *C. sinensis*, *C. australasica*, and *A. buxifolia* were identified using the hmmsearch program of HMMER (version 3.3.2)⁴⁸ and homology-based BLAST searches using *A. thaliana* SHI/STY full length protein sequences as query. Protein names and accession numbers are provided in [Data S7](#).

The amino acids of SHI/STY family proteins from *A. thaliana*, *L. japonicus*, *P. trichocarpa*, *A. coerulea*, *O. sativa* and *C. sinensis* were aligned with MUSCLE (version 5.3)⁴⁵ with default parameters, followed by phylogenetic tree construction with IQTREE (version 1.6.12)⁴⁶ using the maximum-likelihood method. The resulting phylogenetic tree was visualized with R package ggtree (version 3.99.2).⁴⁷ Phylogenetic relationships of *C. sinensis*, *C. australasica*, and *A. buxifolia* were inferred using the Neighbor-Joining method implemented on MEGA7 after alignment using MUSCLE with default parameters.⁴⁴ Numbers next to the branches represent bootstrap support values (1000 replicates).

Subcellular localization

The *Ti3* coding sequence was cloned into the pEarleyGate 104 vector to generate an N-terminal YFP fusion under the control of the CaMV 35S promoter (35S:YFP-*Ti3*). The 35S:YFP-*Ti3* construct and a 35S:YFP control were introduced into *A. tumefaciens* (strain GV3101) and co-infiltrated into *Nicotiana benthamiana* leaves with a nuclear marker (35S:H2B-RFP). Confocal imaging was carried out on a Leica TCS SP8 microscope (Leica, Germany), using excitation/emission settings of 514 nm/525–545 nm for YFP and 552 nm/590–640 nm for RFP.

Multiple sequence alignment of *Ti3* homologs

We identified putative *Ti3* homologs in *C. sinensis*, *C. australasica*, and *A. buxifolia* with highly similar coding sequences. As *T. trifolia* lacks a genome reference, its *Ti3* homolog was obtained via PCR amplification using primers designed from the *C. sinensis* sequence and confirmed by Sanger sequencing. The resulting protein sequences were aligned using the MUSCLE algorithm in MEGA7 and visualized with GeneDoc software.

Dual-luciferase assays

Effector constructs were generated by cloning full-length coding sequences of *Ti3*, *CsFD*, and *CsCEN* into the *Bbs* I linearized pCambia1300 vector under the control of the CaMV 35S promoter. For the *Ti3*-VP64 and *Ti3*-SRDX effectors, the *Ti3* coding sequence was fused to sequences coding VP64 activation domain (49 aa) or SRDX repression domain (12 aa) in-frame before cloning into pCambia1300 vector. The *Ti3*^{24aa}-VP64 effector was generated by cloning the *Ti3*^{24aa} coding sequence (amplified from the *ti3*#2 mutant) in-frame with the VP64 activation domain into the pCambia1300 vector. The promoters of *Ti1* (2474 bp), *Ti2* (2188 bp), and *Ti3* (2358 bp), along with their truncated fragments were PCR amplified from Carrizo citrange genomic DNA. These fragments were inserted into the pGreenII0800-LUC vector (*Bam*H I and *Kpn* I sites) upstream of a *mini*35S promoter (a 60-bp fragment) driving the firefly luciferase reporter gene. All binary vectors were introduced into *A. tumefaciens* strain GV3101 (pSoup) (WEIDI, Shanghai, China). All primers used are listed in [Data S6](#).

The *Agrobacterium* suspensions containing the effector or reporter constructs were mixed in 1:1 ratio to a final OD₆₀₀ of 0.4 and co-infiltrated into *N. benthamiana* leaves. For luminescence imaging, infiltrated leaves were sprayed with D-Luciferin substrate and visualized using In Vivo Plant Imaging System (NightSHADE L985). For quantitative analysis, firefly and renilla luciferase activities were measured using a Dual-luciferase Reporter Assay System (Promega, USA).

DNA affinity purification sequencing (DAP-seq)

The coding sequence of *Ti3* was cloned into a pFN19K HaloTag T7 SP6 Flexi expression vector. The HaloTag-*Ti3* fusion protein was expressed using the TNT SP6 Coupled Wheat Germ Extract System (Promega) following the manufacturer's specifications. Expressed protein was subsequently captured using Magne Halo Tag Beads (Promega).

For the DAP-seq assay, protein-bound beads were incubated with 50 ng of adapter-ligated genomic DNA fragments. After incubation, the beads were washed three times and bound DNA was eluted in 30 μ L of elution buffer. Eluted DNA was prepared into sequencing libraries following the manufacturer's protocol (Illumina) and sequenced on an Illumina NovaSeq platform. Negative control mock DAP-seq libraries were prepared identically but without the addition of fusion protein.

Raw sequencing data were processed using fastp software default parameters to obtain high-quality clean reads.⁵³ These reads were mapped to the sweet orange reference genome (*Citrus sinensis* v2.0 CPBD, http://citrus.hzau.edu.cn/data/Genome_info/SWO.v2.0/SWO.v2.0.genome.fa) using Bowtie2.⁴⁹ Duplicate reads were removed by Picard, and uniquely mapped read were filtered for a MAPQ score > 15 using SAMtools.⁵⁵ Peak calling was performed with MACS2,⁵⁰ *de novo* motif discovery was conducted by HOMER,⁵¹ and peak annotation was carried out with ChIPseeker.⁵²

Transcriptome analysis

Young thorns (stage 9–11) and the associated stems of *P. trifoliata*, shoot apices (around 0.5 cm long shoot apex, including shoot apical meristem, young leaves, young thorns, stems, and axillary buds) of Carrizo citrange WT and mutants (*ti3*, *cscen* *ti3*) were used for total RNA extraction by RNA extraction kit (R4165-02, MAGEN BIOTECH, China) according to the manufacturer's protocol. Sequencing libraries were constructed using a PCR-based protocol and sequenced on an Illumina NovaSeq platform (Novogene, China), generating 150 bp paired-end reads. Raw reads were quality-controlled using fastp (version 0.23.4)⁵³ with default parameters. The resulting clean reads were then mapped to the reference genome (*Citrus sinensis* v2.0 CPBD) using HISAT2.⁵⁴ Transcript abundance was quantified in TPM (Transcripts per million) using StringTie.⁵⁴ Differentially expressed genes (DEGs) were identified using DEseq2.⁵⁶ Heatmaps were generated using R package pheatmap (version 1.0.13). Gene expression values were standardized by row-wise Z-score normalization. DEGs were listed in [Data S1](#) and [S3](#).

Electrophoretic mobility-shift assays (EMSA)

The full-length coding sequence of *Ti3* was cloned into the *Bam*H I and *Sal* I digested pGEX4T-1 vector by Gibson Assembly and introduced into the *Escherichia coli* strain Rosetta (DE3) (WEIDI, China). Recombinant protein GST-*Ti3* or GST tag alone were induced in 500 mL culture with 0.5 mM isopropyl- β -D-thiogalactopyranoside (IPTG) at 20°C for 12 h. Cells were harvested by centrifugation, resuspended in PBS buffer (PH 7.4) with 1 mM PMSF, and lysed by sonication. The soluble fraction was isolated by centrifugation and purified using glutathione-sepharose affinity chromatography. 5' 6-carboxyfluorescein (6-FAM)-labeled double-

stranded DNA probes containing WT or mutant *T1/2/3* promoter elements were synthesized. The 6-FAM-labeled DNA probes with varied CTAG copy numbers were designed based on promoter regions of *T1/3* (F1, F4, F5) and *T1/1* (F2, F3). Unlabeled probes of identical sequence were used as competitors at 10× molar excess. Binding reactions were performed according to the previous method.⁵⁹ Binding reaction mixtures were then loaded onto a 6% native polyacrylamide gel and electrophoresed at 100 V for 70 min at 4°C. Fluorescent signals were visualized using an Amersham Imager 600 (GE Healthcare). All probes used are listed in [Data S6](#).

Quantitative real-time PCR (QRT-PCR)

To analyze the expression pattern of *T1/3*, total RNA was extracted from various tissues, including shoot apices, young thorns, branch buds, stems, roots, leaves and flowers using HiPure HP Plant RNA Mini kit (R4165-02, MAGEN BIOTECH, China) with DNase I treatment to remove genomic DNA. cDNA was synthesized by using the HiScript II 1st Strand cDNA Synthesis Kit with gDNA wiper (R212, Vazyme, China).

Total RNA used for RNA-seq (from young thorns and stems of *P. trifoliata*, and shoot apices of WT and *ti3* Carrizo citrange) was also subjected to reverse transcription for cDNA synthesis. The differential expression of key genes revealed by RNA-seq was further confirmed by qRT-PCR: *T1/1*, *T1/2*, *MYB62*, and *NST1* were analyzed in young thorns versus stems (*P. trifoliata*), and *T1/1*, *T1/2*, and *T1/3* were analyzed in WT versus the *ti3* mutant (Carrizo citrange). Expression pattern of the *T1/3* homologs was also analyzed in thorns and stems (Australian finger lime, Chinese box orange, and lime berry). qPCR reactions were prepared using ChamQ SYBR qPCR Master Mix (Q421, Vazyme, China) and quantified by Roche LightCycler 480 instrument II. *CsActin* was used as a reference gene and relative expression values were calculated using a $2^{-\Delta\Delta Ct}$ method. Three independent biological replicates were performed.

RNA *in situ* hybridization

RNA *in situ* hybridization in *Citrus* were performed as described previously.⁶⁰ The complete coding sequences of *T1/3* and *CsWUS* were used to generate the antisense and sense labelled probes. Shoot apices of Carrizo citrange, Australian finger lime, Chinese box orange, lime berry, and the mutants were fixed and used for hybridizations. Primers used for this experiment are listed in [Data S6](#).

Scanning electron microscopy (SEM)

To examine thorn outgrowth, the apices of WT and mutant plants were dissected to expose the meristem by removing leaf primordia at stages 3–7. The samples were fixed in 2.5% (v/v) glutaraldehyde solution at 4°C, dehydrated in a graded ethanol series, and dried using a Bal-Tec critical point dryer (Leica). Subsequently, they were mounted to stubs, sputter-coated with platinum, and imaged using a Hitachi cold-field emission SEM S-4700-II (Hitachi, Japan).

QUANTIFICATION AND STATISTICAL ANALYSIS

For gene expression analysis by qRT-PCR, three biological replicates were assayed.

For transactivation assay in *N. benthamiana*, three or four independent biological experiments were performed.

All statistical analyses were performed using GraphPad Prism 10 software (<https://www.graphpad-prism.cn/>). Pairwise comparisons were conducted by Student's t-test, multiple comparisons were conducted by one-way ANOVA with Tukey's post hoc test.